High Voltage

Research Article

IET Journals
The Institution of Engineering and Technology

Electromagnetic modelling using T-A formulation for high-temperature superconductor (RE)$Ba_2Cu_3O_x$ high field magnets

eISSN 2397-7264
Received on 28th May 2019
Revised 11th November 2019
Accepted on 10th December 2019
E-First on 6th February 2020
doi: 10.1049/hve.2019.0120
www.ietdl.org

Yawei Wang[1], Hongyu Bai[2] ✉, Jianwei Li[3], Min Zhang[1], Weijia Yuan[1]

[1]*Department of Electronic and Electrical Engineering, University of Strathclyde, Glasgow, G1 1XQ, UK*
[2]*National High Magnetic Field Laboratory, Florida State University, FL 32310, Tallahassee, USA*
[3]*Engineering Science, University of Oxford, Oxford, OX1 3PJ, UK*
✉ *E-mail: bai@magnet.fsu.edu*

Abstract: Second generation (2G) high-temperature superconductor (HTS) (RE)$Ba_2Cu_3O_x$ (REBCO) shows a great potential in building high field magnets beyond 23.5 T. The electromagnetic modelling is vital for the design of HTS magnet, however, this always suffers the challenge of huge computation for high field magnets with large number of turns. This study presents a novel electromagnetic modelling based on T-A formulation for REBCO magnets with thousands of turns. An equivalent turn method is proposed to reduce the number of turns in calculation, so that the computation cost can be reduced significantly, and meanwhile the key electromagnetic behaviour of HTS magnet can be simulated with enough accuracy. The ramping operation of a fully HTS magnet with 12,000 turns are analysed using both the original T-A model with actual turns and improved T-A model with equivalent turns. The two models show a good agreement on the key electromagnetic behaviours of the magnet: distribution of current density, magnetic fields, screen current induced field and magnetisation loss, so that this improved T-A model using equivalent turns is validated. The T-A modelling of REBCO magnet is a powerful tool for the electromagnetic analysis of industry-scale high field magnets.

1 Introduction

Superconducting high field magnet plays an important role in scientific instruments, accelerator magnets, nuclear magnetic resonances and energy storage, which always prefer higher magnetic fields [1–4]. Current superconducting magnets are based on low-temperature superconductors (LTS) like NbTi and Nb3Sn, and their fields are limited to 23.5 T, which is the critical fields of Nb3Sn. The second generation (2G) high-temperature superconductor (HTS), (RE)$Ba_2Cu_3O_x$ (REBCO), shows significant advantages on high critical fields and high current density, which has been improved in recent two decades [5, 6]. It has a great potential to generate extra high magnetic fields up to 100 T at low temperature far exceeding the possible field range of LTS can reach [7]. Therefore, REBCO conductor is also called high field superconductor [8, 9]. Significant process has been achieved on HTS high field magnets in recent 5 years: 32 T field was achieved in 2017 by a LTS/HTS hybrid magnet with a 17 T REBCO insert and 15 T LTS outset in National High Magnetic Field Laboratory (NHMFL), USA [9–11]. A 24 T LTS/HTS hybrid magnet with 9 T insert HTS magnet was developed by the Chinese Academy of Sciences in 2015 [12–16]. Then a 26 T full REBCO magnet was developed by MIT and SuNAM in 2016 [17]. More ambitious HTS magnet projects beyond 30 T have been announced at several institutes in recent 3 years [18, 19].

An efficient numerical modelling tool is vital to study and predict electromagnetic behaviours of HTS magnets, especially the screen current and AC loss. However, numerical modelling of HTS magnet has always suffered the challenges of highly non-linear E–J power relationship, high aspect ratio of coated conductor and hard convergence [20–25]. REBCO high field magnet often consists of thousands of turns, which makes the modelling much more difficult because of the huge computation. Some analytical methods have been developed to calculate the screen current in superconductor, which is simple and fast [26–29]. However, these methods cannot do a comprehensive electromagnetic analysis on the HTS, and are also not suitable for complex electromagnetic environments and operations. Finite-element method (FEM) based on H-formulation has been widely applied on the electromagnetic modelling of HTS applications [30–33], and homogenous H-formulation model has been developed to reduce the computation cost [34, 35]. Its governing equation uses magnetic intensity H as solution variable, and the whole model can be built and solved in commercial FEM software Comsol Multi-physics. T-w model has also been developed for the electromagnetic modelling of HTS, which couples T-formulation (Faraday's law) and integration equation (Biot-Savart Law) [36–39].

A new T-A formulation model has been developed for REBCO conductors in 2016, which is based on the previous T-w model [40]. The key feature of T-A formulation model is to neglect the thickness of REBCO conductors and treat it as thin shell, meanwhile keep the dimension of all the other domains, then apply a T-formulation model on the superconducting shell with lower dimension, and apply an A-formulation model on all the domains. This can significantly reduce the computation cost because of dimension and variables reduction, which makes it possible and easy to complicate electromagnetic modelling of HTS applications [41–45]. However, for high field magnets using REBCO tapes, T-A model still suffers the problem of huge computation, especially for magnets with thousands of turns. Too huge computation can significantly reduce the practicability and convergence of the HTS electromagnetic modelling.

This paper presents an improved T-A model for REBCO high field magnets with large number of turns, which can significantly reduce computation cost, and therefore make the electromagnetic simulation of high field magnets fast, easy and practical. This model is partly inspired by the conventional homogenous H-formulation model, and some techniques and fundamentals of homogenous H-formulation are introduced. The actual turns on the inner part of the pancake coils are replaced with equivalent turns whose number is much less than that of these actual turns. The equivalent turns can significantly reduce the number of meshes as well as computation cost, and meanwhile keep all the key electromagnetic characteristics of the REBCO coil, such as

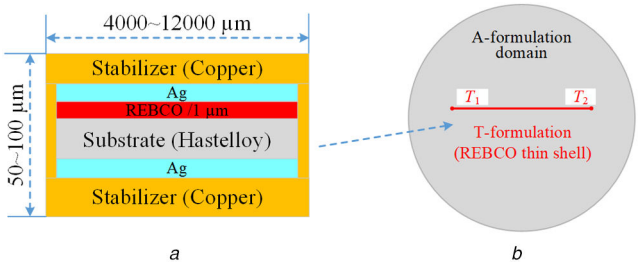

Fig. 1 *Schematic illustration of T-A formulation model*
(a) Schematic illustration of the cross-section of REBCO conductors, ***(b)*** Domain relationship of T-formulation and A-formulation in T-A model

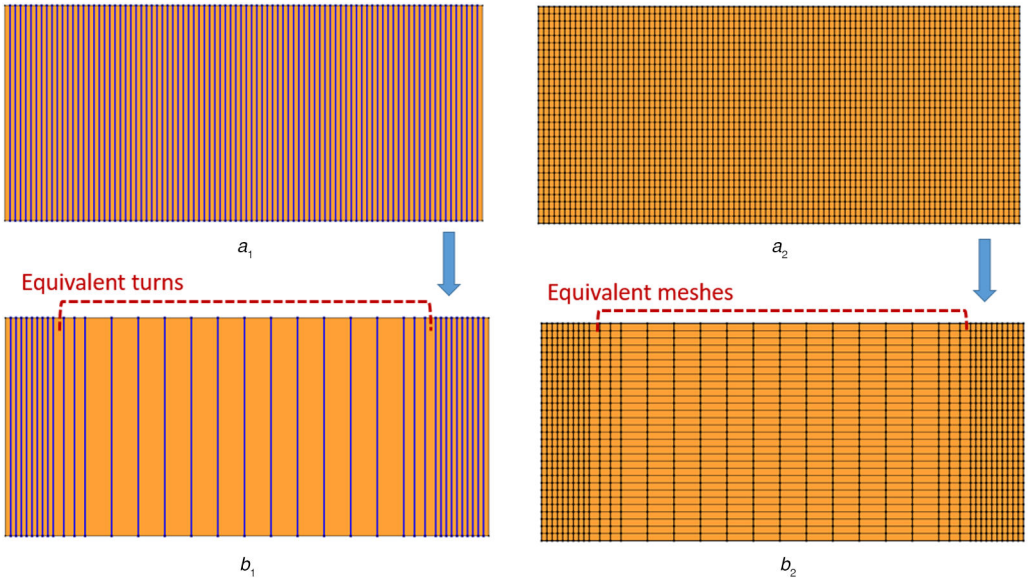

Fig. 2 *2D axisymmetric T-A models for pancake coils using REBCO tapes*
(a_1) Geometry of normal T-A model, ***(a_2)*** Meshes of the original T-A model, ***(b_1)*** Geometry of improved T-A model using equivalent turns, ***(b_2)*** Meshes of improved T-A model using equivalent turns

distribution of current density, magnetic field induced, ramping loss and screen current induced field (SCIF). Then, to validate this model, case comparisons are conducted on a 15 T REBCO magnet with more than 10,000 turns, and key electromagnetic characteristics of these high field magnets are analysed.

2 Numerical model

2.1 T-A formulation

The REBCO coated conductor has a multilayer structure, and the thickness of the superconducting layer is <1% of the total thickness, as shown in Fig. 1*a*. Since the ramping of high field magnets is relatively slow, current only flows in superconducting layer below critical current. Therefore, the metallic layers are neglected in the electromagnetic modelling below critical current. Meanwhile, it is reasonable to treat the REBCO conductor as thin shell considering the high aspect ratio of superconducting layers, as shown in Fig. 2 [37, 40]. The key feature of T-A formulation is to apply the T-formulation on this REBCO thin shell only to calculate the current distribution, and meanwhile apply the A-formulation on all the domains to calculate magnetic fields induced, as shown in Fig. 1*b* [40, 41]. T is the current vector potential. Current flowing in the thin shell does not have component normal to the shell surface, thus current vector potential only has the normal component on the shell. Therefore, the current in thin shell $\boldsymbol{J}$ can be expressed as

$$\boldsymbol{J} = \nabla \times (T\boldsymbol{n}) \tag{1}$$

where T is the normal component of the current vector potential, $\boldsymbol{n} = [n_x, n_y, n_z]$ is the unit normal vector of the thin shell. The governing equations of the T-A model are

$$\begin{cases} \nabla \times \boldsymbol{E}(\boldsymbol{J}) = \dfrac{\partial \boldsymbol{B}}{\partial t}, & \text{on REBCO shell only} \\ \nabla \times \nabla \times \boldsymbol{A} = \mu \boldsymbol{J}, & \text{on all the domain} \end{cases} \tag{2}$$

where $\boldsymbol{A}$ is magnetic potential, $\boldsymbol{B}$ is magnetic flux density, $\boldsymbol{E}$ is electric field. In the T-formulation, the transport current is imposed by adding a Dirichlet boundary condition on the edges of the REBCO shell [40]

$$T_1 - T_2 = \frac{I_{op}}{d} \tag{3}$$

where I_{op} is the transport current, d is the thickness of the REBCO tape (1 μm in this study). T_1 and T_2 are the current vector potential on the two edges of the REBCO shell, as shown in Fig. 1*b*. The current distribution obtained from the T-formulation is input into A-formulation as external current. Therefore, a Neumann boundary condition is added on the REBCO shell in the A-formulation model

$$\boldsymbol{n} \times (\boldsymbol{B}_1 - \boldsymbol{B}_2) = \mu \boldsymbol{J} \tag{4}$$

where μ is the permeability, $\boldsymbol{J}$ is current density obtained from T-formulation, $\boldsymbol{B}_1$ and $\boldsymbol{B}_2$ are the magnetic fields on the two sides of the REBCO shell. The magnetic fields obtained from A-formulation will be fed back to the T-formulation equations. The T-A model is solved in commercial FEM software COMSOL Multiphysics. The T-formulation model is solved in a PDE module, and the A-formulation model is solved in magnetic field module.

E–J power law is applied on the REBCO shell to represent the critical state of HTS

$$\boldsymbol{E}(\boldsymbol{J}) = E_0\left(\frac{|\boldsymbol{J}|}{J_c(\boldsymbol{B})}\right)^{n-1}\frac{\boldsymbol{J}}{J_c(\boldsymbol{B})} \tag{5}$$

where $n = 28$, $E_0 = 1\ \mu$V/cm, J_c is the critical current density. Its field dependence is expressed by following formulas in this study, which is suitable for high fields [46]

$$\begin{cases} I_c(B,\theta) = a_0 B^{-\alpha_0} + \dfrac{a_1 B^{-\alpha_1} - a_0 B^{-\alpha_0}}{w-1}(wF-1) \\ F = (w^2\cos^2\theta + \sin^2\theta)^{-0.5} \\ w = C[B + C^{-(1/\eta)}]^{(1/\eta)} \end{cases} \tag{6}$$

where B is magnetic field norm, θ is the field angle related to c-axis of the tape. More details about these formulas have been presented in reference.

2.2 Modelling of REBCO pancake coils

The electromagnetic fields of REBCO pancake coils show a 2D axisymmetric distribution, thus it can be simulated by a 2D axisymmetric FEM model [47, 48]. As shown in Fig. $2a_1$, the REBCO shell is a line without thickness in the 2D axisymmetric model, on which the T-formulation and superconducting characteristics are applied. There is little current sharing between superconducting layer and metallic layers below critical current, thus these domains can be treated as air in simulation. The distance between adjacent REBCO lines is the average thickness of REBCO tapes. In 2D T-A models for REBCO pancake coils, meshing of A-formulation module seems similar with that of traditional H-formulation model, as shown in Fig. $2a_2$. Superconducting domains (RBECO lines) are meshed to shorter segments, whose dimension is lower than that in H-formulation model. This can significantly reduce computation cost. The number of meshes in T-A model is approximately proportional to the number of turns, as shown in Fig. $2a_2$. High field magnets using REBCO pancake coils often have hundreds of turns, and therefore always suffer the challenges of huge computation cost even if for T-A models.

In REBCO pancake coils, the distributions of magnetic fields and current density show sharply variations on turns near the inner side and outer side of the coil, but have very flat variation on the middle turns of the coil. It is reasonable to apply coarse meshes on the turns with same computational accuracy, which is the fundamental mechanism of previous homogenous H-formulation [34]. In this study, we improve the T-A model by replaying the actual turns on middle zones with equivalent turns, as shown in Fig. $2b_1$. The number of equivalent turns is much less than that of physical turns, thus the number of meshes is significantly reduced, as shown in Fig. $2b_2$. Equivalent critical current $I_{c,\,\mathrm{eq}}$ and transport current $I_{op,\,\mathrm{eq}}$ is applied on these equivalent turns

$$\begin{cases} I_{c,\mathrm{eq}} = n_t I_c \\ I_{op,\mathrm{eq}} = n_t I_{op} \end{cases} \tag{7}$$

where I_c and $I_{op}$are the critical current and transport current of physical turns replaced. n_t is number of physical turns replaced, which is 2–10 in this study. It can increase with the number of physical turns of pancake coils. Therefore, this technique can prevent the increase of computation cost with number of turns of HTS magnets, and therefore, make the electromagnetic modelling of large REBCO magnet system more practical and easier.

3 REBCO magnet for analysis

A 15 T test coil using insulated REBCO tapes has been designed as insert magnet in a high magnetic magnet. This REBCO coil consists of 40 single pancake coils (SPC), and each coil has 300 turns, thus it has 12,000 turns in total. The above model proposed will be validated by simulating the electromagnetic behaviour of this magnet during ramping operations. The mechanical stress analysis on this coil is not considered in this paper. Parameters of the REBCO tape used are based on tape of Superpower. Its width and thickness are 4.1 and 0.1 mm, respectively. Thickness of its superconductor layer is 1 μm. This magnet is designed to generate 15 T magnetic fields at axial centre, with transport current 200 A which is well below the critical current of the Superpowers's tape of the art-of-state. More specifications of this magnet are shown in Table 1. As shown in Fig. 3, only upper half of the magnet (20 SPCs) is calculated in the simulation, considering the symmetric characteristics of electromagnetic fields. All the pancake coils are named SPC1–SPC40 from top coil to the bottom coil. The actual number of turns in original T-A model is 6000, and it is reduced to 1560 turns by applying the equivalent turn method, as shown in Fig. 3. Table 2 shows the comparison between the original T-A models with actual turns and the improved T-A model with equivalent turns. For A-formulation, the coil domains are meshed with quadrilateral elements, as shown in Figs. $2a_2$ and b_2; other domains are meshed with triangular elements. For T-formulation, each REBCO line is meshed to 30 fine segments. Both T-formulation and A-formulation use linear interpolation functions. In the simulation, the operating current of this HTS magnet is 200 A, and it is ramped up and down with ramping rate 1 A/s, as shown in Fig. 4. Note that only the HTS coil is ramped in this study, the background field is not considered. The solution time is significantly reduced by applying the equivalent turns, as shown in Table 2.

Table 1 Specification of the 15 T REBCO magnet studied

Parameter	REBCO Magnet
inner/outer diameter	60/120 mm
height	174 mm
number of pancakes	40
gap between pancakes	0.25 mm
turns per pancake	300
width/thickness of tape	4.1/0.1 mm
total tape length	3393 m
operating temperature	4 K
operating current	200 A
central fields per ampere	75 mT/A
self-inductance	4.18 H

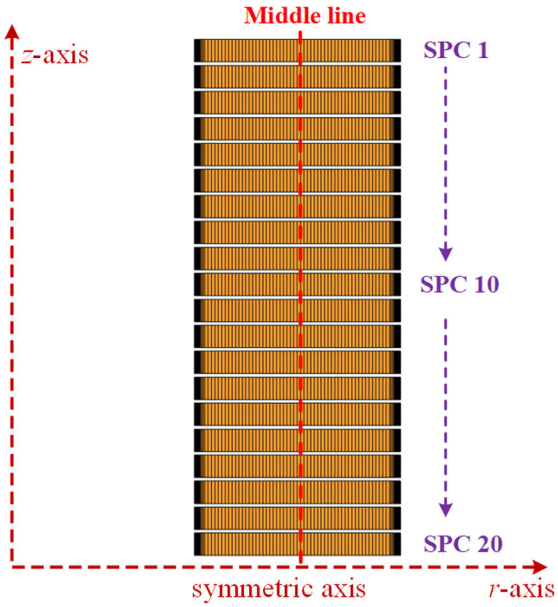

Fig. 3 *2D axisymmetric T-A models for REBCO magnet with multiple coils*

Table 2 Specification of the 15 T REBCO magnet studied

Parameter	Original T-A model	Improved T-A model
number of turns calculated	6000	1560
number of elements	241,545	80,183
interpolation function	linear	linear
n-value	28	28
number of DOF	397,419	112,472
solution time of a ramp up to 200 A (CPU I7-8700)	4 h	1 h

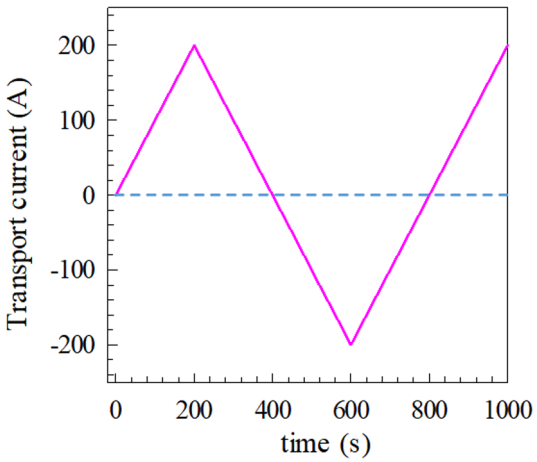

Fig. 4 *Transport current of the magnet during the ramping up and down operation, ramping rate 1 A/s*

4 Results and discussion

4.1 Distribution of current and fields

Same ramping operation is simulated by both original T-A model with actual turns and improved T-A model with equivalent turns. The H-formulation model, which is most popular electromagnetic modelling method of HTS, is also applied on the magnet here to validate the T-A model. Fig. 5 shows the distribution of magnetic field (parallel component to the tape and perpendicular component to the tape) when the magnet is ramped up to 200 A for the first time, $t = 200$ s. The result from T-A models matches well with that from H-formulation model, which validates the correctness of the T-A model. The overall profile from improved T-A model agrees well with that from original T-A model at each pancake coil. The only difference is that the colour of improved T-A model seems brighter than that of original T-A model. This is because the original T-A model with actual turns has much more black lines (REBCO shell) than the improved T-A model with equivalent turns. These black lines reduce the brightness of the picture. This does not mean that the magnetic field in Figs. 5a_1 and $a2$ are lower than that of Figs. 5$b1$ and $b2$. Fig. 6 shows distribution of the normalised current density J/J_c at $t = 200$ s. In T-A models, only the REBCO lines without thickness have current, and there is no current on other domains. For a better presentation, the current line is plot as tube with enlarged thickness. The overall profile of original T-A model is well reproduced by the improved T-A model with equivalent turns. There is a slight difference on the transferring zones between actual turns and equivalent turns, as shown in Fig. 6. This is led by position difference between actual turns and equivalent turns, which induces a slight difference on the distribution of magnetic fields. The normalised current from both T-A models shows a same distribution among turns with that from H-formulation, which validates the correctness of both T-A models. The results in Fig. 6 also show that coils near the top and bottom of the magnet have much more penetration than the coils near the middle zones of the magnet. This is because the coils on top and bottom have much higher radial background fields, which are perpendicular to the tape surface. This generates two effects: first, due to the anisotropy of critical current of REBCO tapes, the tapes of top coils have lower critical current, and radial magnetic field has more penetration on the superconductors. Second, higher radial fields induce more screen current on superconducting layers because of more flux coupling. The main component of magnetic fields on middle coils is axial field, which is parallel to the tapes surface. This parallel field is hard to induce screen current in superconducting layers of REBCO tape because of its thin thickness (1 μm). Both effects lead to much more penetration on top coils. Figs. 5 and 6 only show the top six pancakes of the magnet, where the distribution of fields and current shows a more significant variation among pancakes. In the other pancakes, the current and fields of original T-A model are also accurately reproduced by the improved T-A model.

Fig. 7 shows the distribution of current density magnitude on the middle turns of each pancake coil, which matches the red dashed line in Fig. 3. Note that the real current density in the equivalent turns of improved T-A model is n_t ($n_t = 5$ in this study) times of that in the original T-A model, since the transport current and critical current have been enlarged n_t times in these equivalent turns, as shown in (7). In Fig. 7, the data from improved T-A model has been shrank to $1/n_t$ of its calculated value for a better comparison. Results from T-A improved model show a good agreement with that from original model. Generally, the current density magnitude increases from the middle coils to the top coils, due to the increases of radial fields, which leads to relatively low current density on middle coils (like SPC 30). However, the top coil (SPC 1) also has a lower current density magnitude than others because it has lower critical current. Small oscillations occur on the virgin zone of the tape, where should have no current. This is induced by numerical errors in solution, and same situations have also occurred on H-formulations [32].

4.2 Screen current induced field

Screen currents are induced by the radial fields, part of them are opposite to the transport current, as shown in Figs. 5 and 6. SCIF can lead to significant reduction and non-uniformity on magnetic fields, which is a great challenge for many high field magnet applications like MRI/NMR and accelerator [49–51]. Fig. 8 shows the distribution of magnetic fields at $t = 400$ s, when the magnet is ramped down to 0 A for the first time. There is a considerable field residue (up to 4.6 T) on the REBCO coils when the transport current is ramped down to zero. Fig. 9 shows the normalised current density at $t = 400$ s. Although the total transport current of each turn is zero at $t = 400$ s, there are several screen currents with

opposite direction in each tape, which generate the magnetic fields in Fig. 8. Higher radial fields at top coils induce much more screen currents, which generate higher SCIF on these coils. This screen current also generates a residual field 0.5 T at the centre of the magnet though the transport current is 0 A at the same time.

Here we also calculated the magnetic field induced by the magnet without screen current, which has a uniform current distribution in all the tapes. The field difference ΔB at magnet centre is used to represent the influence of SCIF

$$\Delta B = B_{SC} - B_{uniform} \quad (8)$$

where B_{SC} is the magnetic field at magnet centre considering the screening current. $B_{uniform}$ is the magnetic field at magnet centre with uniform current density distribution, which is accurately proportional to the transport current. Fig. 10 shows the dependence of this field difference ΔB on the central magnetic field induced by uniform current density $B_{uniform}$, which is used to represent the

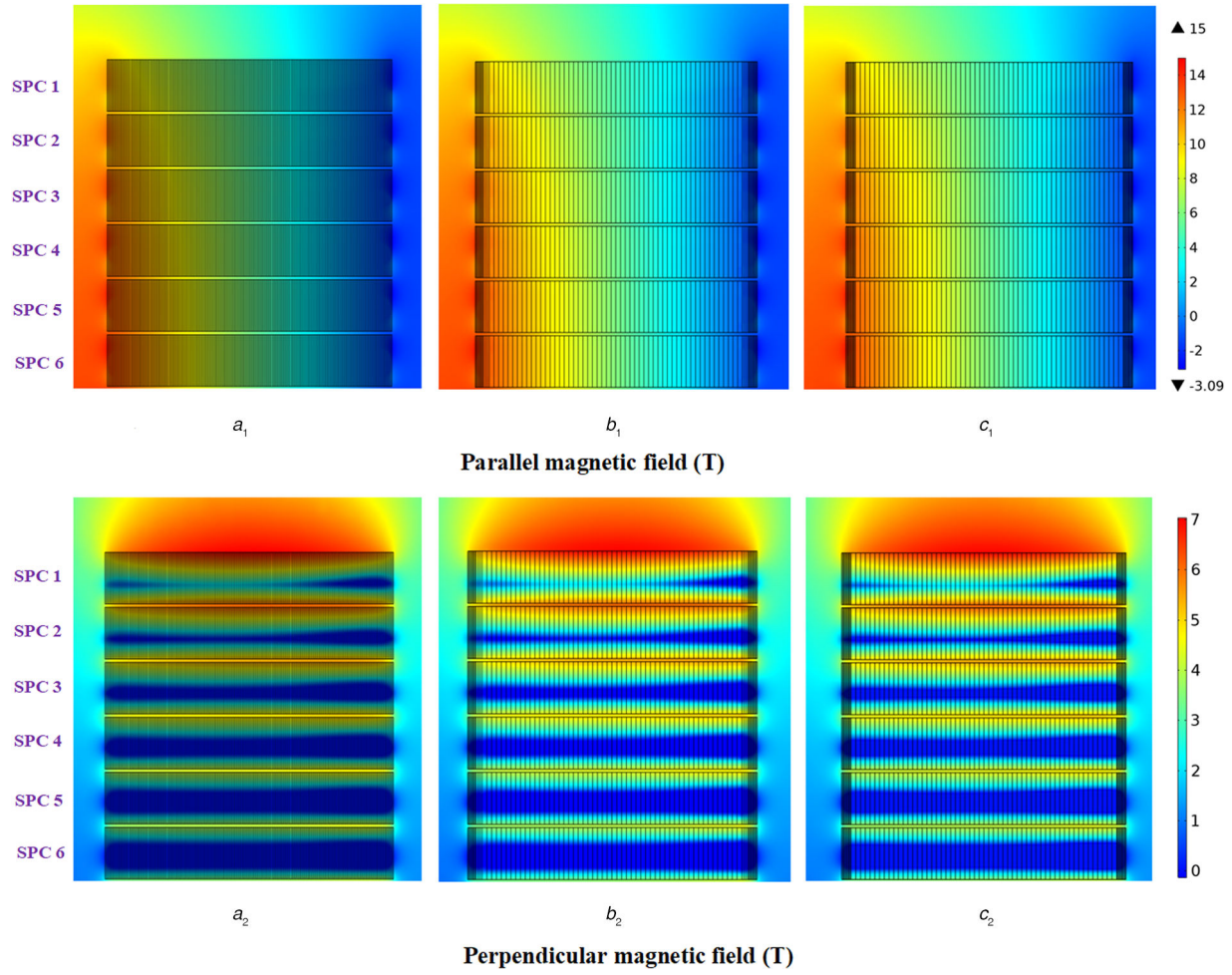

Fig. 5 *Distribution of magnetic fields norm ||B|| when the transport current is ramped up to 200 A for the first time (t = 200 s). Notice that only the top 6 pancakes are plot here, where the magnetic field have a significant variation; the following 14 pancakes are not shown*
(a1), (a2) Original T-A model, ***(b1), (b2)*** Improved T-A model, ***(c1), (c2)*** H-formulation model

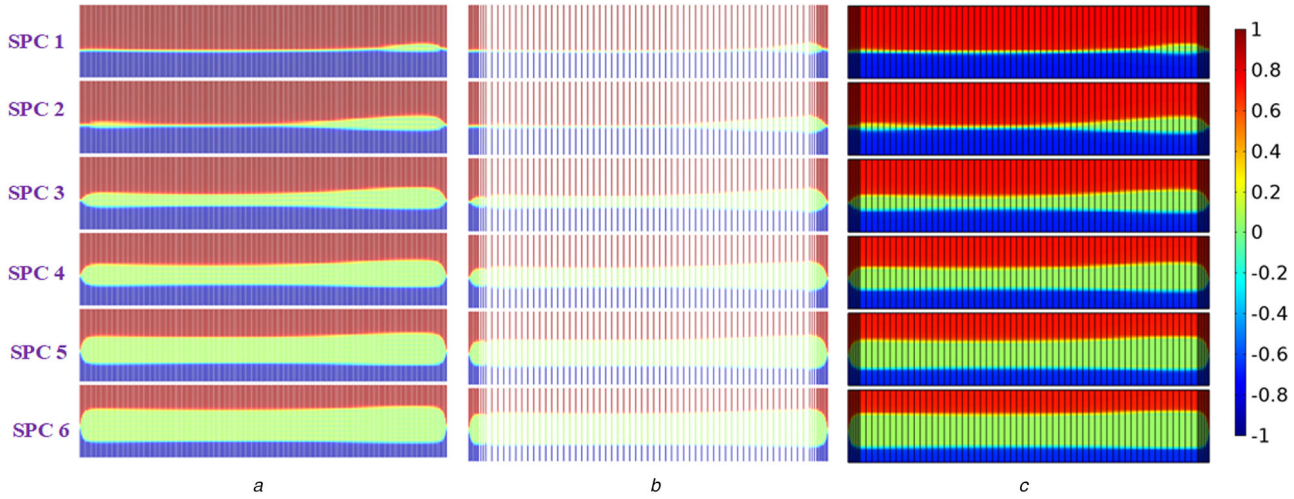

Fig. 6 *Normalised current density J/J_c when the transport current is ramped up to 200 A for the first time (t = 200 s)*
(a) Original T-A model for the magnet with actual turns, ***(b)*** Improved T-A model with equivalent turns. Note that current on superconducting shell (line) without thickness is plotted as tube with thickness for better visualisation

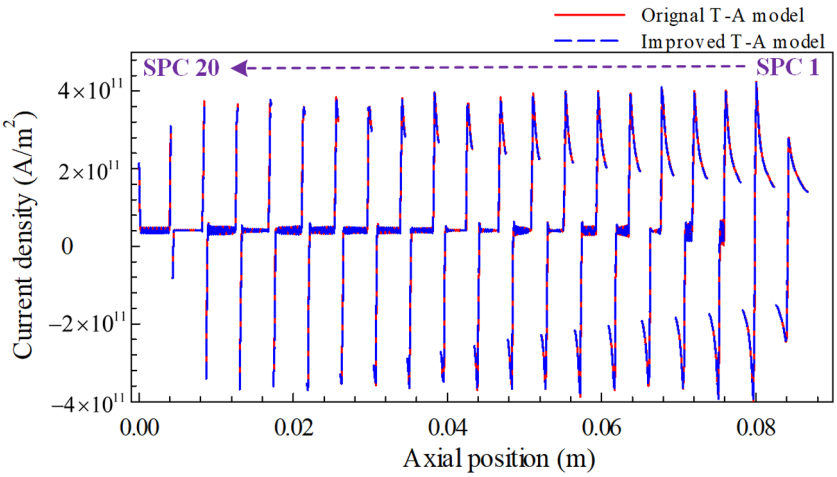

Fig. 7 *Current density J on the middle turns of each pancakes (red dashed middle line in Fig. 3) when the transport current is ramped up to 200 A for the first time, t = 200 s*

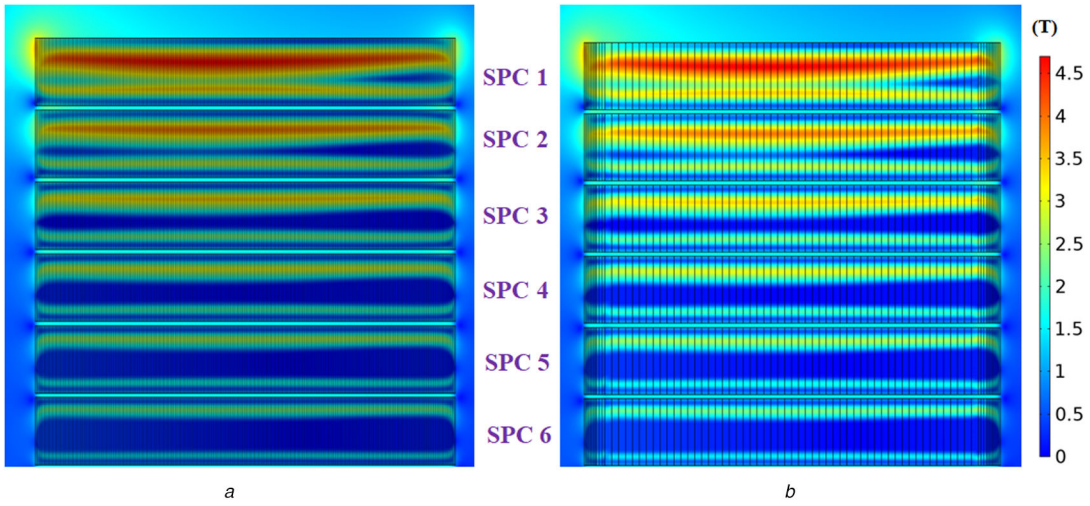

Fig. 8 *Distribution of magnetic fields norm ||B|| when the transport current is ramped down to 0 A for the first time (t = 400 s)*
(a) Original T-A model, ***(b)*** Improved T-A model

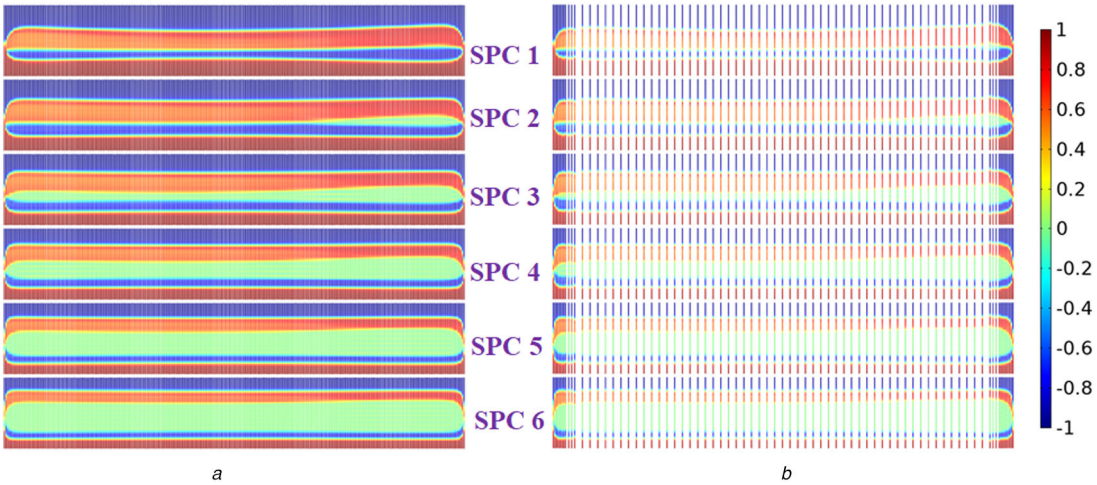

Fig. 9 *Normalised current density J/Jc when the transport current is ramped down to 0 A for the first time (t = 400 s)*
(a) Original model with actual turns, ***(b)*** Improved T-A model with equivalent turns. Note that current on superconducting shell (line) without thickness is plotted as tube with thickness for better visualisation

SCIF. During the ramping cycle, the variation of transport current is as shown in Fig. 4. Significant magnetic hysteresis is observed during the ramping up and down operations of HTS magnet, which is induced by SICF. The field reduction induced by SCIF can be ~0.9 T under transport current 200 A. Measures have to be developed to eliminate or reduce the SCIF, which will be discussed in future publications.

The results in Figs. 8–10 show that, for the study of SCIF in HTS magnet, the improved T-A model with equivalent turns can reproduce accurately the data of original T-A model with actual turns, like distribution of current density, magnetic fields and magnetic hysteresis induced by SCIF.

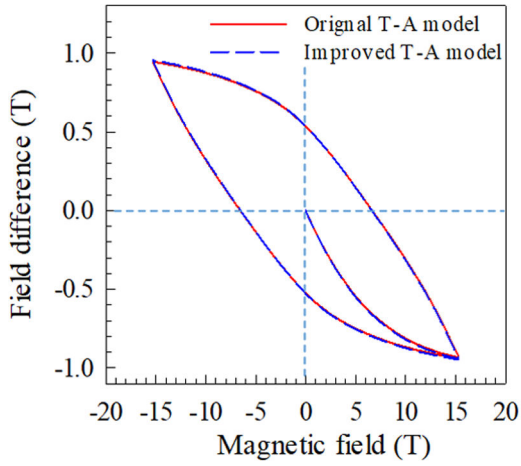

Fig. 10 *Influence of SCIF during the ramping up and down cycles: x-axis is the central magnetic field of the magnet with uniform current density on REBC tapes, y-axis is the central field difference* ΔB *defined in (8)*

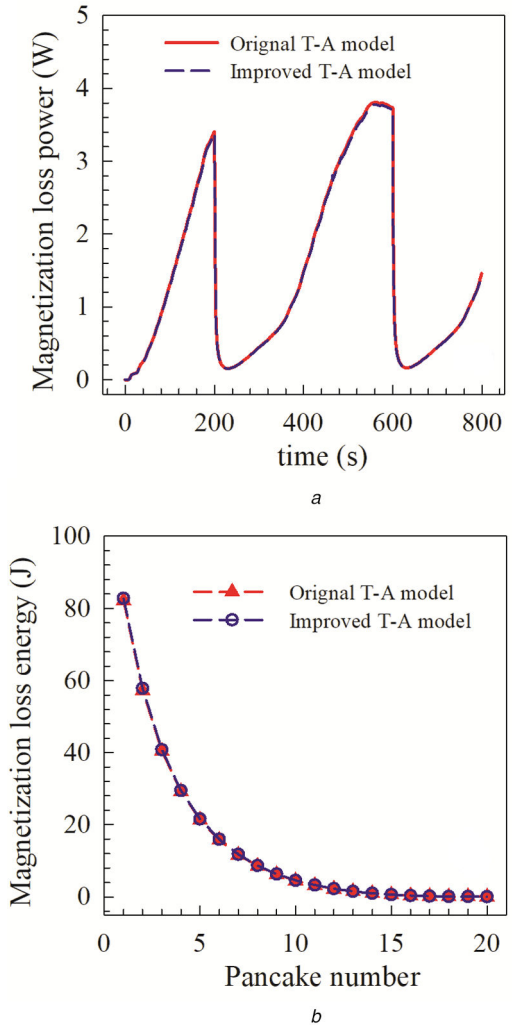

Fig. 11 *Magnetisation loss of the 20 SPCs during the ramping up and ramping down operations*

(a) Total magnetisation loss power of the 20 SPCs, ***(b)*** Distribution of the magnetisation loss energy during the first ramping up to 200 A (t = 0–200 s) among pancake coils

4.3 Ramping loss

Magnetisation loss is generated in superconducting layers during the ramping operation of HTS magnet, due to flux creep and jump [52]. This is the main part of ramping loss of HTS magnet below critical current, which may lead to a potential quench and ramp failure [33, 53]. In T-A models, this magnetisation loss can be calculated by

$$\begin{cases} W_m = d\int_l \boldsymbol{E}\cdot\boldsymbol{J}\mathrm{d}l \\ Q_m = \int W_m(t)\mathrm{d}t \end{cases} \tag{9}$$

where W_m and Q_m are the magnetisation loss power and energy, respectively. Fig. 11*a* shows total magnetisation loss power W_m of the 20 pancake coils during the ramping operation in Fig. 4. Fig. 11*b* shows the distribution of total magnetisation loss energy Q_m generated in first ramping up to 200 A among pancake coils. The magnetisation loss shows a significant non-uniform distribution among pancakes. The top coils generate much more loss energy than the middle coils because of much more screen current and flux penetration on top coils. During the first ramping cycle t = 0–200 s, the magnetisation loss power W_m increases fast with the transport current and reach to peak value when the transport current stops increasing at t = 200 s. Then the magnet starts to ramp down and the magnetisation loss power drops fast to nearly zero with the decrease of transport current. However, the valley point does not occur at t = 400 s when the transport current ramp down to 0 A. Due to the magnetic hysteresis induced by screen current, magnetisation loss power drops to valley point at t = 230 s and then increases gradually with the decreases of transport current. It increases continuously in the next ramping up operation to −200 A, and reaches to a higher peak value than the peak of first ramping up at t = 560 s. The accumulation of screen current induces more penetration on the REBCO coils, as shown in Fig. 12. There is a time gap between peak points of magnetisation loss power (t = 560 s) and transport current (t = 600 s), which is also induced by the screen current.

Figs. 11 and 12 show that, for the magnetisation loss generated in the ramping of HTS magnet, the results from improved T-A model with equivalent turns have a good agreement with that from the original T-A model with actual turns.

5 Conclusion

This paper presents an electromagnetic modelling based on T-A formulation for high field magnets using REBCO tapes. To solve the problem of huge computation, an equivalent turn method is proposed for REBCO magnet with large number of turns. This method can considerably reduce the number of turns calculated in solution, prevent the approximately linear increase of meshes with the number of actual turns, and therefore significantly reduce the computation cost, make the electromagnetic modelling of industry-scale HTS high field magnets practical and easy.

This improved T-A model with equivalent turns is validated by comparing its results from original T-A model with actual turns. A REBCO test coil of 15 T consisting of 40 SPCs and 12,000 turns is analysed, and its key characteristics during ramping operation are calculated and compared: distribution of current density and magnetic fields, SCIF and magnetisation loss during ramping. For all these issues, the results from improved T-A model with equivalent turns have a very good agreement with that from original T-A model with actual turns, which validate the feasibility of the improved T-A model with equivalent turns.

The high field magnets consisting of multiple REBCO pancakes always suffer from a serious problem of SCIF, which is induced by radial fields. The SICF can lead to a considerable field reduction on the centre of this magnet, which is 0.9 T for the 15 T magnet studied. It can also induce a high residual field on the magnet when the magnet is fully discharged, 0 A transport current. Highest residual fields often occur on the top and bottom coils of the magnet, which reaches to 4.6 T for this 15 T magnet. This is a potential risk for the mechanical stability and safety of high field magnet, which needs a special attention in the magnet design. The top and bottom coils have higher radial fields than other coils, which induce higher screen current and magnetisation loss on these coils. During the ramping up and down cycle, more magnetisation

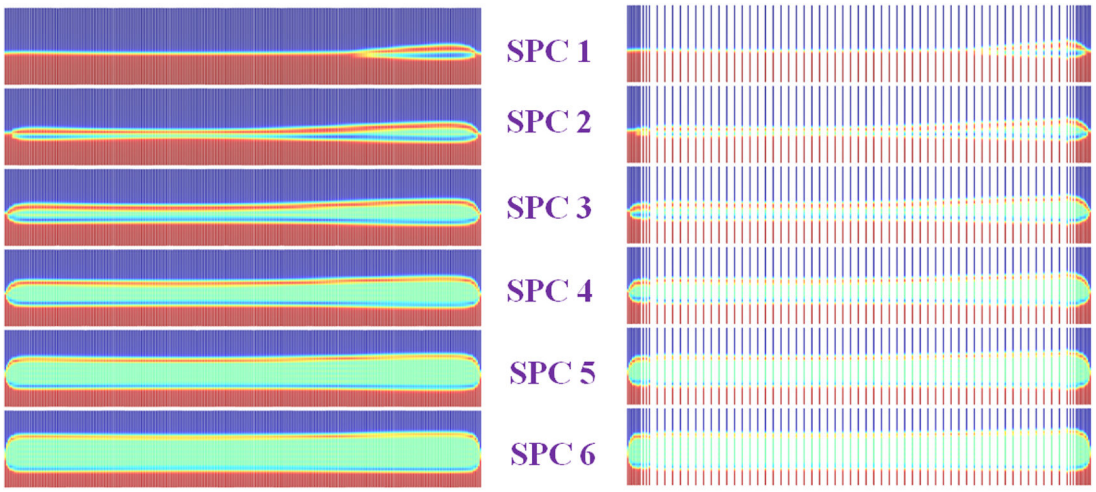

Fig. 12 *Normalised current density J/Jc at t = 560 s*

(a) Original model with actual turns, ***(b)*** Improved T-A model with equivalent turns. Note that current on superconducting shell (line) without thickness is plotted as tube with thickness for better visualisation

loss is generated in superconductors after the first ramping up operation, which is induced by screen currents.

6 Acknowledgments

Dr Yawei Wang thank the support of European Union's Horizon 2020 research and innovation programme under the Marie Sklodowska-Curie grant agreement no. 799902. This work was supported in part by the National Natural Science Foundation of China under grant nos. 11802036 and 11872195. This work was also partially performed at the National High Magnetic Field Laboratory, which was supported by the U.S. National Science Foundation Cooperative Agreement no. DMR-1644779 and the State of Florida.

7 References

[1] Hahn, S., Kim, K., Kim, K., *et al.*: '45.5-Tesla direct-current magnetic field generated with a high-temperature superconducting magnet', *Nature*, 2019, **570**, pp. 496–499

[2] Usoskin, A., Betz, U., Gnilsen, J., *et al.*: 'Long-length Ybco coated conductors for ultra-high field applications: gaining engineering current density via pulsed Laser deposition/alternating beam-assisted deposition route', *Supercond. Sci. Technol.*, 2019, **32**, (9), p. 094005

[3] Qu, T., Michael, P.C., Bascuñán, J., *et al.*: 'Test of an 8.66-T rebco insert coil with overbanding radial build for a 1.3-ghz lts/hts nmr magnet', *IEEE Trans. Appl. Supercond.*, 2017, **27**, (4), pp. 1–5

[4] Li, J.W., Yang, Q.Q., Robinson, F., *et al.*: 'Design and test of a new droop control algorithm for a Smes/battery hybrid energy storage system', *Energy*, 2017, **118**, pp. 1110–1122

[5] Zhao, Y., Zhu, J.M., Jiang, G.Y., *et al.*: 'Progress in fabrication of second generation high temperature superconducting tape at Shanghai superconductor technology', *Supercond. Sci. Technol.*, 2019, **32**, (4), p. 044004

[6] Gao, P.F., Wang, X.Z.: 'Analysis of torsional deformation-induced degeneration of critical current of Bi-2223 hts composite Tapes', *Int. J. Mech. Sci.*, 2018, **141**, pp. 401–407

[7] Iwasa, Y., Hahn, S.: 'First-cut design of an all-superconducting 100-T direct current magnet', *Appl. Phys. Lett.*, 2013, **103**, (25), p. 253507

[8] Schwartz, J.: 'Viewpoint: are No-insulation magnets a paradigm shift for high-field Dc superconducting magnets?', *Supercond. Sci. Technol.*, 2016, **29**, (5), p. 050501

[9] Weijers, H.W., Markiewicz, W.D., Gavrilin, A.V., *et al.*: 'Progress in the development and construction of a 32-T superconducting magnet', *IEEE Trans. Appl. Supercond.*, 2016, **26**, (4), pp. 1–7

[10] Breschi, M., Cavallucci, L., Ribani, P.L., *et al.*: 'Analysis of quench in the nhmfl rebco prototype coils for the 32 T magnet project', *Supercond. Sci. Technol.*, 2016, **29**, (5), p. 055002

[11] Berrospe-Juarez, E., Zermeño, V.M.R., Trillaud, F., *et al.*: 'Estimation of losses in the (Re)Bco two-coil insert of the nhmfl 32 T all-superconducting magnet', *IEEE Trans. Appl. Supercond.*, 2018, **28**, (3), pp. 1–5

[12] Wang, Q., Liu, J., Song, S., *et al.*: 'High temperature superconducting ybco insert for 25 T full superconducting magnet', *IEEE Trans. Appl. Supercond.*, 2015, **25**, (3), pp. 1–5

[13] Liu, J.H., Dai, Y.M., Li, L.K.: 'Progress in the development of a 25 T all superconducting nmr magnet', *Cryogenics*, 2016, **79**, pp. 79–84

[14] Wang, L., Wang, Q., Li, L., *et al.*: 'The effect of winding conditions on the stress distribution in a 10.7 T Rebco insert for the 25.7 T superconducting magnet', *IEEE Trans. Appl. Supercond.*, 2018, **28**, (3), pp. 1–5

[15] Li, L., Cheng, J., Cui, C., *et al.*: 'Numerical analysis of mechanical behavior for a 9.\4-T whole-body mri magnet', *IEEE Trans. Appl. Supercond.*, 2017, **27**, (4), pp. 1–5

[16] Li, Y., Wang, Q.L., Wang, L., *et al.*: 'Electromagnetic design of a 16–9 T high field double superconducting magnets system for nuclear demagnetization refrigerator', *IEEE Trans. Appl. Supercond.*, 2017, **27**, (4), pp. 1–5

[17] Yoon, S., Kim, J., Lee, H., *et al.*: '26t 35 mm all-Gdba2cu3o7-X multi-width No-insulation superconducting magnet', *Supercond. Sci. Technol.*, 2016, **29**, (4), p. 04LT04

[18] Liu, J.H., Wang, Q.L., Dai, Y.M., *et al.*: 'A 15-T rebco insert for a 30-T all superconducting magnet', *IEEE Trans. Appl. Supercond.*, 2017, **27**, (4), pp. 1–5

[19] Kim, K., Bhattarai, K.R., Jang, J.Y., *et al.*: 'Design and performance estimation of a 35 T 40 Mm No-insulation all-rebco user magnet', *Supercond. Sci. Technol.*, 2017, **30**, (6), p. 065008

[20] Pardo, E., Kapolka, M.: '3d magnetization currents, magnetization loop, and saturation field in superconducting rectangular prisms', *Supercond. Sci. Technol.*, 2017, **30**, (6), p. 064007

[21] Wang, Y., Wan Kan, C., Schwartz, J.: 'Self-protection mechanisms in No-insulation (Re)Ba 2cu 3o X high temperature superconductor pancake coils', *Supercond. Sci. Technol.*, 2016, **29**, (4), p. 045007

[22] Gömöry, F., Sheng, J.: 'Two methods of Ac loss calculation in numerical modelling of superconducting coils', *Supercond. Sci. Technol.*, 2017, **30**, (6), p. 064005

[23] Zhang, M., Coombs, T.A.: '3d modeling of high-tcsuperconductors by finite element software', *Supercond. Sci. Technol.*, 2012, **25**, (1), p. 015009

[24] Wang, Y., Song, H., Xu, D., *et al.*: 'An equivalent circuit grid model for No-insulation hts pancake coils', *Supercond. Sci. Technol.*, 2015, **28**, (4), p. 045017

[25] Wan Kan, C., Masson, P.J., Luongo, C., *et al.*: 'Three-dimensional micrometer-scale modeling of quenching in high-aspect-ratio coated conductor Tapes-part I: model development and validation', *IEEE Trans. Appl. Supercond.*, 2010, **20**, (6), pp. 2370–2380

[26] Wang, L., Wang, Q., Liu, J., *et al.*: 'Screening current-induced magnetic field in a noninsulated gdbco hts coil for a 24 T all-superconducting magnet', *IEEE Trans. Appl. Supercond.*, 2017, **27**, (4), pp. 1–6

[27] Yang, D.G., Kim, K.L., Choi, Y.H., *et al.*: 'Screening current-induced field in non-insulated gdbco pancake coil', *Supercond. Sci. Technol.*, 2013, **26**, (10), p. 105025

[28] Yanagisawa, Y., Nakagome, H., Koyama, Y., *et al.*: 'Effect of current sweep reversal on the magnetic field stability for a Bi-2223 superconducting solenoid', *Physica C*, 2009, **469**, (22), pp. 1996–1999

[29] Koyama, Y., Takao, T., Yanagisawa, Y., *et al.*: 'Towards beyond 1ghz nmr: mechanism of the long-term drift of screening current-induced magnetic field in a Bi-2223 coil', *Phys. C*, 2009, **469**, (13), pp. 694–701

[30] Hong, Z., Campbell, A.M., Coombs, T.A.: 'Numerical solution of critical state in superconductivity by finite element software', *Supercond. Sci. Technol.*, 2006, **19**, (12), pp. 1246–1252

[31] Zhang, M., Kvitkovic, J., Kim, C.H., *et al.*: 'Study of 2 g high temperature superconducting coils: influence of anisotropic characteristics', *J. Appl. Phys.*, 2013, **114**, (4), p. 043901

[32] Xia, J., Bai, H., Lu, J., *et al.*: 'Electromagnetic modeling of rebco high field coils by theh-formulation', *Supercond. Sci. Technol.*, 2015, **28**, (12), p. 125004

[33] Wang, Y.W., Zhang, M., Yuan, W.J., *et al.*: 'Non-uniform ramping losses and thermal optimization with turn-to-turn resistivity grading in a (Re) $Ba_2cu_3o_x$ magnet consisting of multiple No-insulation pancake coils', *J. Appl. Phys.*, 2017, **122**, (5), p. 053902

[34] Zermeno, V.M.R., Abrahamsen, A.B., Mijatovic, N., *et al.*: 'Calculation of alternating current losses in stacks and coils made of second generation high temperature superconducting Tapes for large scale applications', *J. Appl. Phys.*, 2013, **114**, (17), p. 173901
[35] Berrospe-Juarez, E., Zermeño, V.M.R., Trillaud, F., *et al.*: 'Iterative multi-scale method for estimation of hysteresis losses and current density in large-scale hts systems', *Supercond. Sci. Technol.*, 2018, **31**, (9), p. 095002
[36] Amemiya, N., Miyamoto, K., Murasawa, S.-I., *et al.*: 'Finite element analysis of Ac loss in non-twisted Bi-2223 tape carrying Ac transport current and/or exposed to Dc or Ac external magnetic field', *Phys. C*, 1998, **310**, (1), pp. 30–35
[37] Amemiya, N., Murasawa, S.-I., Banno, N., *et al.*: 'Numerical modelings of superconducting wires for Ac loss calculations', *Phys. C*, 1998, **310**, (1), pp. 16–29
[38] Ueda, H., Saito, J., Ariya, Y., *et al.*: 'Reduction of irregular magnetic field generated by screening current in rebco coil', *IEEE Trans. Appl. Supercond.*, 2015, **25**, (3), pp. 6603205
[39] Okabe, Y., Honda, T., Kajikawa, K.: 'Numerical reproduction of screening-current-induced fields in hts tape windings using finite element method', *J. Phys., Conf. Ser.*, 2017, **871**, pp. 012047
[40] Zhang, H., Zhang, M., Yuan, W.: 'An efficient 3d finite element method model based on the T–a formulation for superconducting coated conductors', *Supercond. Sci. Technol.*, 2016, **30**, (2), p. 024005
[41] Liang, F., Venuturumilli, S., Zhang, H., *et al.*: 'A finite element model for simulating second generation high temperature superconducting coils/stacks with large number of turns', *J. Appl. Phys.*, 2017, **122**, (4), p. 043903
[42] Yawei, W., Min, Z., Francesco, G., *et al.*: 'Study of the magnetization loss of corc® cables using a 3d T-a formulation', *Supercond. Sci. Technol.*, 2019, **32**, (2), p. 025003
[43] Zhu, Z., Wang, Y., Venuturumilli, S., *et al.*: 'Influence of harmonic current on magnetization loss of a triaxial corc rebco cable for hybrid electric aircraft', *IEEE Trans. Appl. Supercond.*, 2018, **28**, (4), pp. 1–5
[44] Wang, Y., Zheng, J., Zhu, Z., *et al.*: 'Quench behavior of high-temperature superconductor (Re)Ba2cu3o X corc cable', *J. Phys. D: Appl. Phys.*, 2019, **52**, (34), p. 345303
[45] Zhu, Z., Wang, Y., Xing, D., *et al.*: 'Quench of a single-layer rebco corc cable with non-uniform terminal contact resistance', *IEEE Trans. Appl. Supercond.*, 2019, **29**, (5), pp. 1–5
[46] Hilton, D.K., Gavrilin, A.V., Trociewitz, U.P.: 'Practical fit functions for transport critical current versus field magnitude and angle data from (Re)Bco coated conductors at fixed low temperatures and in high magnetic fields', *Supercond. Sci. Technol.*, 2015, **28**, (7), p. 074002
[47] Zhang, M., Kvitkovic, J., Kim, J.H., *et al.*: 'Alternating current loss of second-generation high-temperature superconducting coils with magnetic and non-magnetic substrate', *Appl. Phys. Lett.*, 2012, **101**, (10), p. 102602
[48] Wang, Y., Song, H., Yuan, W., *et al.*: 'Ramping turn-to-turn loss and magnetization loss of a No-insulation (Re) $Ba_2cu_3o_x$ high temperature superconductor pancake coil', *J. Appl. Phys.*, 2017, **121**, (11), p. 113903
[49] Iguchi, S., Piao, R., Hamada, M., *et al.*: 'Advanced field shimming technology to reduce the influence of a screening current in a rebco coil for a high-resolution Nmr magnet', *Supercond. Sci. Technol.*, 2016, **29**, (4), p. 045013
[50] Min Cheol, A., Jeongwoo, J., Woo Seung, L., *et al.*: 'Experimental study on hysteresis of screening-current-induced field in an Hts magnet for Nmr applications', *IEEE Trans. Appl. Supercond.*, 2014, **24**, (3), pp. 1–5
[51] Zhang, M., Yuan, W., Hilton, D.K., *et al.*: 'Study of second-generation high-temperature superconducting magnets: the self-field screening effect', *Supercond. Sci. Technol.*, 2014, **27**, (9), p. 095010
[52] Zhenan, J., Wei, Z., Quan, L., *et al.*: 'The dynamic resistance of ybco coated conductor wire: effect of Dc current magnitude and applied field orientation', *Supercond. Sci. Technol.*, 2018, **31**, (3), p. 035002
[53] Lu, J., Choi, E.S., Kandel, H., *et al.*: 'Hysteresis loss of rebco conductor up to 35 T', *IEEE Trans. Appl. Supercond.*, 2014, **24**, (3), pp. 8200104